Journal of Structural Geology, Vol. 15, No. 7, pp. 819 to 830, 1993
Printed in Great Britain

0191-8141/93 $06.00+0.00
© 1993 Pergamon Press Ltd

The brittle–ductile transition in porous sedimentary rocks: geological implications for accretionary wedge aseismicity

JIAXIANG ZHANG,* DAN M. DAVIS and TENG-FONG WONG

Department of Earth and Space Sciences, State University of New York, Stony Brook, NY 11794, U.S.A.

(*Received* 20 *December* 1991; *accepted in revised form* 17 *August* 1992)

Abstract—Thrusting earthquakes in subduction zones generally occur along only part of the plate boundary, with motion along the shallowest part of the plate boundary occurring aseismically. The maximum size of subduction boundary thrust earthquakes depends strongly upon the down-dip width of the seismogenic zone. The single most uncertain factor in determining that width is the location of the up-dip limit of the zone (the seismic front), which depends upon the mechanical state of the sedimentary rocks in the plate boundary zone. In order to come to a better understanding of the seismic potential of sediments in a subduction zone, we carried out a series of triaxial experiments on Berea and Kayenta sandstones. Based on our experimental data, a brittle–ductile transition map was constructed showing that both porosity and effective pressure are important factors controlling the transition from brittle to macroscopically ductile behavior in porous rocks. In the brittle field, a sample fails by shear localization on one slip plane accompanied by strain softening and dilatancy, whereas in the ductile field, a sample deforms homogeneously with a constant yield stress or slight hardening. By comparing such a map with the estimated porosity profile of an accretionary wedge, the likely nature and rough location of the boundary between brittle and ductile behavior can be inferred. If the sediments along a plate boundary are too young and undercompacted to be capable of brittle shear localization, then their deformation is likely to be aseismic. In this way, it may be possible for even a very broad fore-arcs to produce no great earthquakes. However, great earthquakes are to be expected at margins that have large zones of plate contact along which many sediments are compacted and well lithified. Such rocks are expected to be capable of shear localization and brittle failure with the potential for stick–slip behavior.

INTRODUCTION

THE GREATEST and most destructive class of earthquakes consists of those associated with the thrust boundary between the downgoing and overlying plates at subduction zones (e.g. 1960 Chile, 1964 Alaska). The factors that control the maximum size of such earthquakes at a particular margin are not well understood; nor is the relationship between the seismicity and other aspects of the tectonics of a subduction zone. In this paper, we will present laboratory results that suggest a possible explanation for much of the variability in seismic character among modern fore-arcs.

It has been recognized for some time that subduction zones differ greatly in the size and frequency of large and great earthquakes. Margins of the 'Marianas-type', at which both plates are oceanic in character and where there is little or no terrigenous sedimentation, do not produce large earthquakes. These margins are generally characterized by a steeply dipping subduction slab, a predominance of basaltic (vs andesitic) volcanism, a poorly developed flexural outer-rise bulge, back-arc spreading and little or no generation of uplifted terraces but, rather, subsidence (Kanamori 1986). Conversely, at 'Chilean-type' margins, the slab dips more gently, andesitic volcanism is prevalent, and there is a well-developed outer flexural bulge, a lack of back-arc spreading and pronounced uplift terraces. In some cases there is a very well developed fore-arc, with a large accretionary wedge including huge quantities of terrigenous sediments originally deposited in the trench. A number of margins appear to be intermediate between these two classes.

The frontal region of a fore-arc, nearest the trench, is typically occupied by an accretionary wedge, a zone of thin-skinned deformation at which sediments are accreted. A wide variety of soft- and hard-sediment deformational styles have been observed in accretionary wedges (e.g. Lundberg & Moore 1986), but their overall shapes and the orientations of major faults within them are explained quite simply by assuming that they deform in response to the driving and resisting tectonic stresses (e.g. Chapple 1978, Davis *et al.* 1983, Stockmal 1983). The convex cross-sectional taper of the frontal regions of most accretionary wedges is consistent with the idea that strength increases with both depth and distance from the deformation front (Zhao *et al.* 1986). Byrne *et al.* (1988) have pointed out that at several margins the front of the backstop and the location of the outer-arc high are approximately coincident with the trenchward limit of plate-boundary thrusting earthquakes. They suggest that the seismic or aseismic character of a plate boundary may be related to the mechanical character of sediments along that boundary.

Sediments in fore-arcs

It is only very close to the trench that it has been possible to drill entirely through an accretionary wedge in order to sample the rocks at its base. Despite hole-stability problems, drilling during DSDP Leg 78A docu-

*Present address: AMOCO Production Company, Tulsa, OK 74102, U.S.A.

mented both discrete thrust surfaces and zones with pronounced scaly fabrics adjacent to them (Moore *et al.* 1986), and provided indirect evidence for both nearly lithostatic pore-fluid pressures (Moore & Biju-Duval 1984) and migration of the pore fluids (Davis & Hussong 1984). ODP Leg 131 drilling in the front of the Nankai accretionary wedge penetrated completely through the basal décollement zones after having first passed through a significant imbricate thrust. Each of these zones of shear was found to be associated with an anomalous porosity offset (Shipboard Scientific Party 1991), suggesting the possibility that the fault zones are also zones of elevated pore fluid pressure.

However, the vast bulk of the rocks in fore-arcs remain beyond our direct study because of the great depths to which they are buried. For the most part, we are limited to indirect inferences based upon seismic velocities, gravity modeling, and modeling constraints. Recent advances in seismic reflection techniques have permitted the imaging of virtually an entire fore-arc in terms of seismic velocity (Bangs *et al.* 1990). This has made it possible to draw inferences about the porosity and possible overpressuring of the accreted sediments, and hence the mechanical state of parts of a fore-arc that are well beyond the reach of the drill.

The progressive loss of porosity and the attendant increase in the strength of accretionary wedge sediments are likely to occur by a combination of chemical and mechanical processes. Clay dehydration reactions can be an important part of the lithification process, and the water that is released by such processes can contribute to elevated overpressures and retard the compaction process. The weakness of smectites may contribute to the aseismic character of these accretionary wedges to the depth at which they undergo a transition of illites, which are considerably stronger (Vrolijk 1990). The emphasis of our study is upon how the mechanical behavior of porous sediments is influenced by the progressive loss of porosity, and its relations to the seismic or aseismic character of a plate boundary.

Distribution of modern fore-arc seismicity

Our understanding of seismic potential at subduction zones is complicated by the relatively short duration of the period during which there have existed seismometers to permit the recording of earthquakes. It is not always possible to determine whether the absence of instrumentally recorded events at a particular margin indicates that the margin is aseismic or whether it merely reflects the fact that the repeat time between events exceeds the period of instrumental coverage. For example, although great thrust earthquakes have been documented in eastern Makran, it is not clear whether western Makran is devoid of such events or whether it is in an interseismic period of several centuries between great events (Byrne *et al.* in press).

Various workers have sought to determine the factors controlling the maximum size of plate boundary thrust earthquakes at a subduction zone. One interesting approach is to seek empirical relations using observable attributes of subduction that, in a statistical sense, explain much of the variance among them. Ruff & Kanamori (1980) found a fairly strong tendency for great earthquakes to occur where the subduction rate is high and the downgoing plate is young. One possible explanation for such a relation is the tendency for the rapid subduction of young lithosphere to produce a shallowly-dipping slab due to the relatively buoyant character of the slab. Empirical relations, although tantalizing, have thus far failed to provide a really reliable predictor of the seismicity of a margin.

Large earthquakes require large slip areas and therefore extend a considerable distance along strike. The rupture areas of thrust earthquakes at subduction zones generally have along-strike lengths 2–3 times their down-dip widths (e.g. Abe 1975), with the notable exceptions of the 1960 Chile, 1964 Alaska and 1957 Aleutian earthquakes for which the lengths of the rupture zones are each 4–6 times the corresponding widths. Therefore, with due caution because of the unexplained large aspect ratio of some of the greatest earthquakes ever recorded, it can be said that the down-dip width of the seismogenic zone is an important factor influencing the maximum size of earthquakes at most margins (e.g. Byrne *et al.* 1988). If this is the case, then the mechanical state of the sediments along the subduction thrust boundary (which, we argue, determines how much of the plate boundary slip is seismic or aseismic) is important in influencing the seismic character of the plate boundary.

Using teleseismic, local network, and OBS data, Chen *et al.* (1982) found that modern accretionary wedges appear to be aseismic. Byrne *et al.* (1988) surveyed several subduction zones and found that in each case the frontal regions of both the overlying plate and the plate boundary are aseismic. They mapped the location of the frontal extent of small events (the 'seismic front') at each margin where the data were available and found a good correlation between the trenchward limit of small events and the trenchward boundary of the zone of large plate-boundary thrust events.

Previous rock mechanics studies

In order to understand better the deformation mechanisms that control the location of the down-dip limit of the seismogenic zone, where rocks undergo a transition from localized brittle fracture to homogeneous plastic flow, intensive laboratory studies of low-porosity crystalline rocks under elevated confining pressure and temperature have been conducted (e.g. Heard 1960, Edmond & Paterson 1972, Tullis & Yund 1977, Paterson 1978, Fredrich *et al.* 1989, Evans *et al.* 1990).

In contrast, the deformation mechanisms involved in the upper bound of seismicity, where the deformation of porous sediments may play an important role, has received little attention, although laboratory studies of brittle–ductile transition in porous rocks have been conducted to some extent (e.g. Handin *et al.* 1963,

Edmond & Paterson 1972, Jamison & Teufel 1979, Bernabe & Brace 1990, Wong 1990). The brittle–ductile transition in porous rocks is characterized by qualitative changes in both inelastic behavior and failure mode. Similar to the brittle behavior of low porosity rocks, brittle failure in porous rocks also occurs by shear localization, accompanied by strain softening and dilatancy. However, in the ductile field, the deformation involves homogeneously distributed grain-scale microcracking without shear localization. Thus, although the macroscopic behavior is ductile, shearing occurs by processes that, on the grain scale, may be regarded as brittle.

Previous studies have focused on the effect of pressure. It is generally accepted that an increase in confining pressure promotes the transition from brittle to ductile behavior (e.g. Handin *et al.* 1963, Jamison & Teufel 1979, Bernabe & Brace 1990). However, taken by itself, this pressure effect on the brittle–ductile transition observed in laboratories seems inconsistent with the down-dip transition from aseismic to seismic slip beneath the fore-arc (e.g. Byrne *et al.* 1988). This inconsistency suggests that in addition to pressure, there may be other parameters, such as temperature, porosity, grain size, geometry and packing, and a variety of chemical processes that affect the failure modes of sedimentary rocks. In this study, we focus upon porosity which, along with confining pressure, appears capable of explaining the observed failure mode behavior.

It was found (Handin *et al.* 1963) that an increase in the temperature up to 300°C has no significant effect on the overall deformation of porous rocks. Therefore, recent studies (Zhang *et al.* 1987, 1992, Hirth & Tullis 1989, Wong 1990, Scott & Nielsen 1991) have focused on the effect of porosity on the brittle–ductile transition. Our preliminary results show that both pressure and porosity exert important controls over the brittle–ductile transition in porous sandstones and that brittle behavior is promoted by a decrease in porosity and in effective confining pressure. Based upon microstructural observations on Oughtibridge Ganister (7% porosity) deformed under conditions of brittle faulting to ductile deformation, Rutter & Hadizadeh (1991) suggested that ductile deformation was enhanced in rocks with sufficient porosity to allow pore-collapse to occur through crushing and sliding along shear-oriented grain boundaries.

In order to come to a better understanding of the failure mode and the seismic potential of sediments in a subduction zone, we have carried out a series of experiments on Berea and Kayenta sandstones. Our experimental data were then compiled together with data from previous studies (Handin *et al.* 1963, Jamison & Teufel 1979, Jones 1980, Bernabe & Brace 1990) to construct a transition map in a space of effective pressure and porosity. Similar work has then carried out on ODP Leg 131 samples from the Nankai Trough. In the following sections, we describe our experimental results and suggest some implications for the seismotectonics of convergent margins.

EXPERIMENTAL PROCEDURE

The sandstones studied

Two types of sandstones, Berea and Kayenta, were tested in our experiments. Model analyses (Zhang *et al.* 1990a) showed that Berea sandstone is comprised of 75% quartz, 10% feldspar, 5% calcite and 10% clay; Kayenta sandstone is relatively clay-free, consisting of about 81% quartz, 9% orthoclase, 1% calcite and 7% other fragments. The sandstones are well sorted with equant grain shape. The Berea sandstone is highly cemented compared to the Kayenta sandstone. The hydrostatic compaction behaviors of the two sandstones have been studied comprehensively in the laboratory (Zhang *et al.* 1990a,c). The porosities of the Berea sandstone samples studied by different authors (e.g. Handin *et al.* 1963, Jamison & Teufel 1979, Bernabe & Brace 1990) range from 17 to 22% and consequently, the mechanical behavior as a function of effective pressure varies somewhat among the different studies. Our samples obtained from the Cleveland quarry, Ohio, all have porosity values of about 21%. The Kayenta sandstone samples of porosity values of about 21% were kindly supplied by W. F. Brace (Massachusetts Institute of Technology) from the same block studied by Jones (1980). Both sandstones are homogeneous with no bedding plane anisotropy.

Triaxial deformation tests

Our experiments were performed in a servo-controlled triaxial test system at room temperature under constant external confining pressures up to 460 MPa and constant pore pressures of up to 50 MPa. Our test data (Zhang *et al.* 1990a) have suggested that the effective stress law is applicable to the porous sandstones, i.e. the mechanical deformation responses are basically identical under the same effective pressure (confining pressure minus pore pressure). Therefore, in this study, we only report the test data under a constant pore pressure of 10 MPa. The strain rate was about 2.6×10^{-5} s^{-1} which is sufficiently slow for fully 'drained' deformation. Kerosene was used as confining pressure medium.

The sample configuration is shown in Fig. 1. The cylindrical samples, 18.4 mm in diameter and 38.1 mm in length, were saturated with distilled water as pore pressure medium. If the polyolefine jacket were in direct contact with the sample, then the significant elastic mismatch between the deformed sample and the relatively stiff polyolefine would induce a local stress concentration which could result in extensive cracking perpendicular to the sample axis during unloading. To avoid such unloading cracks, we used a sandwiched copper layer between the sample and the polyolefine. Using such a jacketing configuration, the development of high stress concentration in the immediate vicinity of the sample is inhibited by the copper of low yield stress which undergoes high strain by plastic flow.

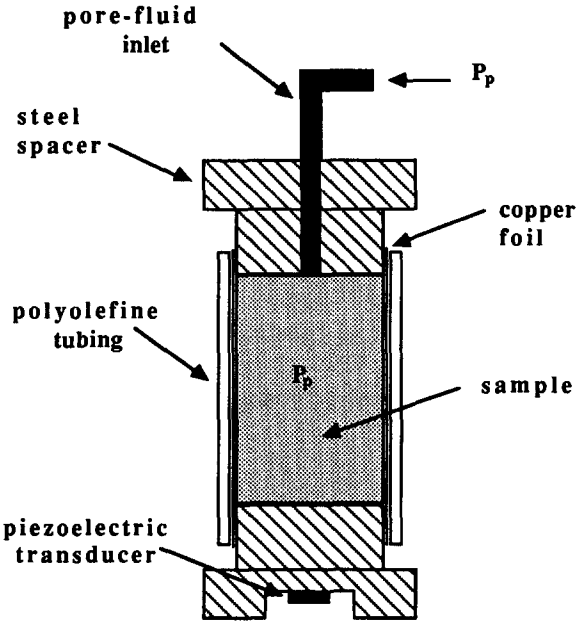

Fig. 1. Sample configuration used in our triaxial tests and AE measurements.

Both confining pressure and pore pressure were monitored by strain-gage pressure transducers to accuracies of 0.5 and 0.125 MPa, respectively. During an experiment in which a sample is subjected to axial loading, the pore volume change in the sample would result in a pore pressure change. A pressure generator was used to compensate for pore volume changes within the sample, keeping the pore pressure constant. The pore volume change, which should be equal to the amount of fluid added to or taken from the sample to maintain constant pore pressure, was recorded by monitoring the piston displacement of the pressure generator with a displacement transducer (DCDT). Porosity change was determined from the pore volume change divided by initial bulk volume of the sample with an uncertainty of 0.1%. The axial load was measured with an external load cell with an accuracy of 1 kN. The displacement was measured outside the pressure vessel with a DCDT installed between the moving piston and the fixed upper platen. The uncertainty of the axial displacement measurement was 10 μm.

The stiffness of the loading system was 2.38×10^8 N m^{-1}. The axial displacement of the sample was obtained by subtracting the elastic displacement from the total displacement recorded by the DCDT. The axial strain was calculated with respect to the initial length of the sample. In the calculation of the axial stress from the recorded axial force, the average change in the cross-sectional area due to the bulging of the deformed sample was taken into account. The relative increase in area was estimated by the difference between the porosity change and the axial strain.

Acoustic emission measurement

As shown in Fig. 1, a piezoelectric transducer (PZT-7, 5.0 mm diameter, 1 MHz longitudinal resonant frequency) was installed to measure AE activity during the triaxial experiments. The PZT transducer was mounted in a hole of 9.0 mm diameter and 4.0 mm depth in a steel spacer attached to the jacketed sample.

The experimental set-up for monitoring and recording AE activity is similar to those of our previous studies (Zhang *et al.* 1990b,c). The AE signals were conditioned by a preamplifier (gain 40 dB, frequency response 1.5 kHz–5 MHz). Electrical noises and spikes were excluded from AE recordings by a discriminator similar to that originally designed by Sondergeld (1980). Two characteristics of the incoming signal were checked by the discriminator. First, the amplified signal had to exceed a threshold level of 30 mV, which is about twice the noise level. Second, it had to persist for a minimum of four cycles at a level above the threshold before the discriminator would generate a single pulse which was recorded by a pulse counter.

EXPERIMENTAL RESULTS

Mechanical deformation

Effect of pressure on the brittle–ductile transition. The changes in differential stress and porosity as a function of axial strain imposed upon samples of Berea sandstone are shown, respectively, in Figs. 2(a) & (b). Figures 3(a) & (b) show the same for Kayenta sandstone. The data for Berea sandstone were obtained at three effective pressures, 40, 250 and 450 MPa, The Kayenta sandstone data were obtained at 20 and 150 MPa. At relatively low effective pressures, 40 MPa for Berea sample BER1 and 20 MPa for Kayenta sample KAY1, a peak deviatoric stress was attained at a relatively small axial strain (less than 2%) beyond which strain softening ensued. Brittle failure occurred by a shear localization fault by about 30° to the loading axis. The porosities of the samples decreased overall during the triaxial deformation. However, a comparison between the hydrostatic compaction curves and the mean stress vs porosity change data of BER1 (Fig. 2d) and KAY1 (Fig. 3c) shows that the porosity changes in the triaxially deformed samples were less than in hydrostatically compacted samples. This indicates that the brittle samples underwent dilatancy during triaxial deformation.

At higher effective pressure, the failure mode became ductile. These samples attained almost constant yield stresses and were deformed homogeneously up to an axial strain more than 25%, as shown by the curves (Figs. 2a & b and 3a & b) for Berea sample BER2 under 250 MPa and Kayenta sample KAY2 under 150 MPa. The samples underwent significant porosity loss. The effect of pressure on the transition to ductile behavior is similar to that previously observed for Berea sandstone (Handin *et al.* 1963, Jamison & Teufel 1979, Bernabe & Brace 1990). However, with further increases in the effective pressure the sample showed strain softening and dilatancy beyond a peak differential stress, as indi-

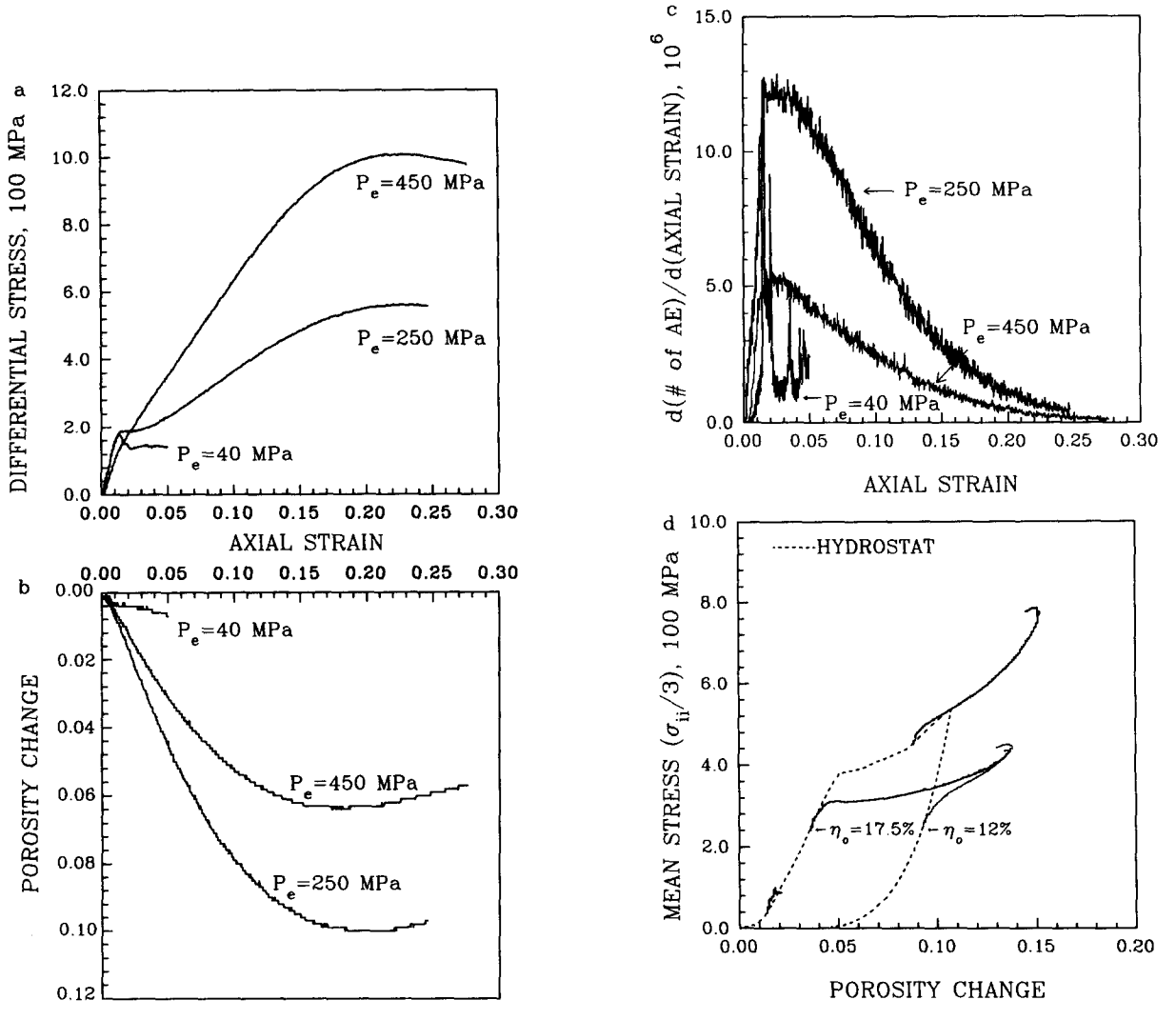

Fig. 2. The stress–strain, porosity change and AE data of Berea sandstone at three effective pressures of 40 (BER1), 250 (BER2) and 450 MPa (BER3): (a) differential stress–axial strain data; (b) porosity change–axial strain data; (c) AE data for Berea sandstone at three effective pressures of 40 (BER1), 250 (BER2) and 450 MPa (BER3); (d) mean effective stress–porosity change data for Berea sandstone. The dashed line is hydrostatic response of Berea sandstone. The solid lines are from triaxial tests. Overconsolidated sample BER4 has an initial porosity of 12% and normal-consolidated sample BER2 has an initial porosity of 17.5% at the effective pressure of 250 MPa.

cated by the data for Berea sample BER3 under an effective pressure of 450 MPa (Figs. 2a & b). A single shear band oriented at approximately 30° to the axial direction was observed after it had been deformed into the post-failure region. Similar behavior for Kayenta sandstone was also observed by Jones (1980) when she performed a triaxial test under an effective pressure of 400 MPa. This phenomenon in which rock samples that behave ductilely in a range of confining pressures become brittle again at high pressures is called 'high pressure embrittlement' (Paterson 1976, Zhang *et al.* 1990b).

Effect of porosity on the brittle–ductile transition. To investigate the effects of porosity, we hydrostatically precompacted samples to a desired porosity (Figs. 2d and 3c). If we define the initial porosity to be the value just before the sample is subjected to a differential stress, then a range of different initial porosities can be obtained in this way at a given effective pressure. For example, as shown in Fig. 3(c), by compacting Kayenta sample KAY2 directly to 150 MPa, a porosity of 17% is obtained, and by compacting sample KAY3 to 540 MPa and then unloading to 150 MPa a porosity of only 11% is obtained. Similarly, two initial porosities of 17.5 and 12% at effective pressure of 250 MPa were obtained by pre-compacting Berea samples BER2 and BER4 to appropriate hydrostatic loading paths (Fig. 2d). Figures 4 and 5 showed how those samples of different initial porosities were deformed with distinct failure modes. The curves of the denser samples of BER4 and KAY3 show that differential stresses initially increase, reaching a peak value, after which strain softening occurred with further deformation. During this latter stage the samples experienced dilatancy. The failure mode was brittle with a shear localization along one slip plane of the samples. On the other hand, the less dense samples of BER2 and KAY2, whose data are also shown in Figs. 2 and 3, deformed ductilely. Therefore, with increasing porosity, the failure modes change from brittle to ductile.

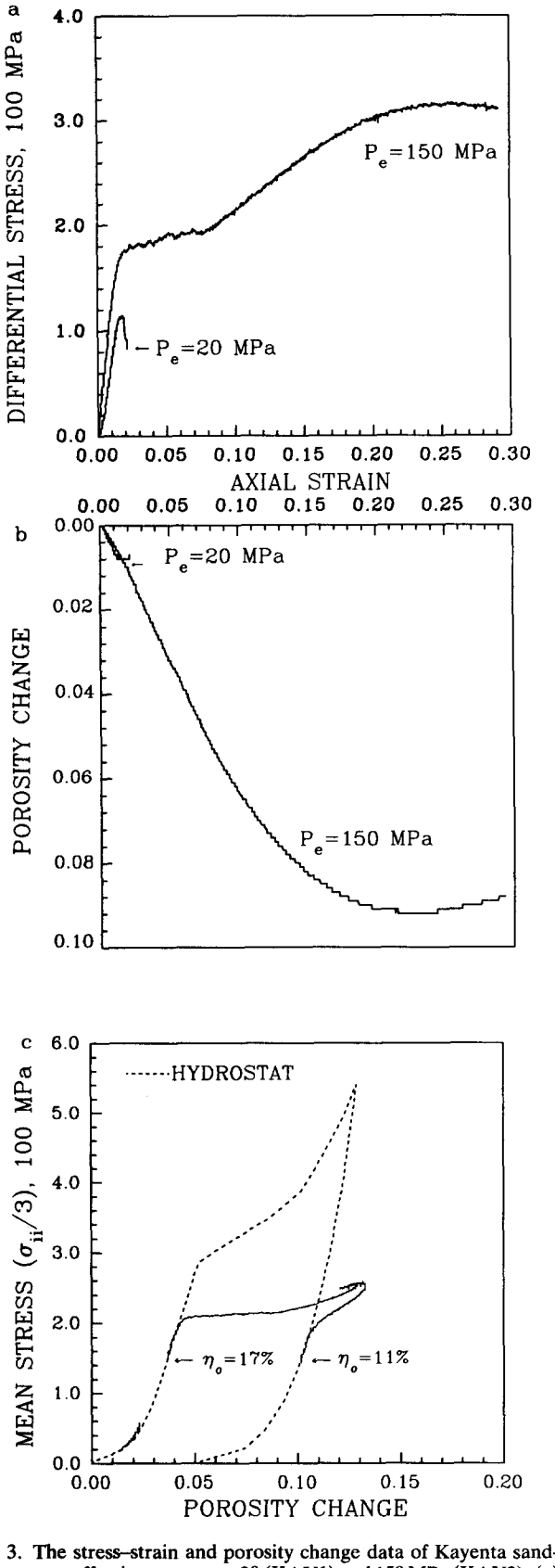

Fig. 3. The stress–strain and porosity change data of Kayenta sandstone at two effective pressures, 20 (KAY1) and 150 MPa (KAY2): (a) differential stress–axial strain data; (b) porosity change–axial strain data; (c) mean effective stress–porosity change data for Kayenta sandstone. The dashed line is the hydrostatic response of Kayenta sandstone. Overconsolidated sample KAY3 has an initial porosity of 11% and normal-consolidated sample KAY2 has an initial porosity of 17%.

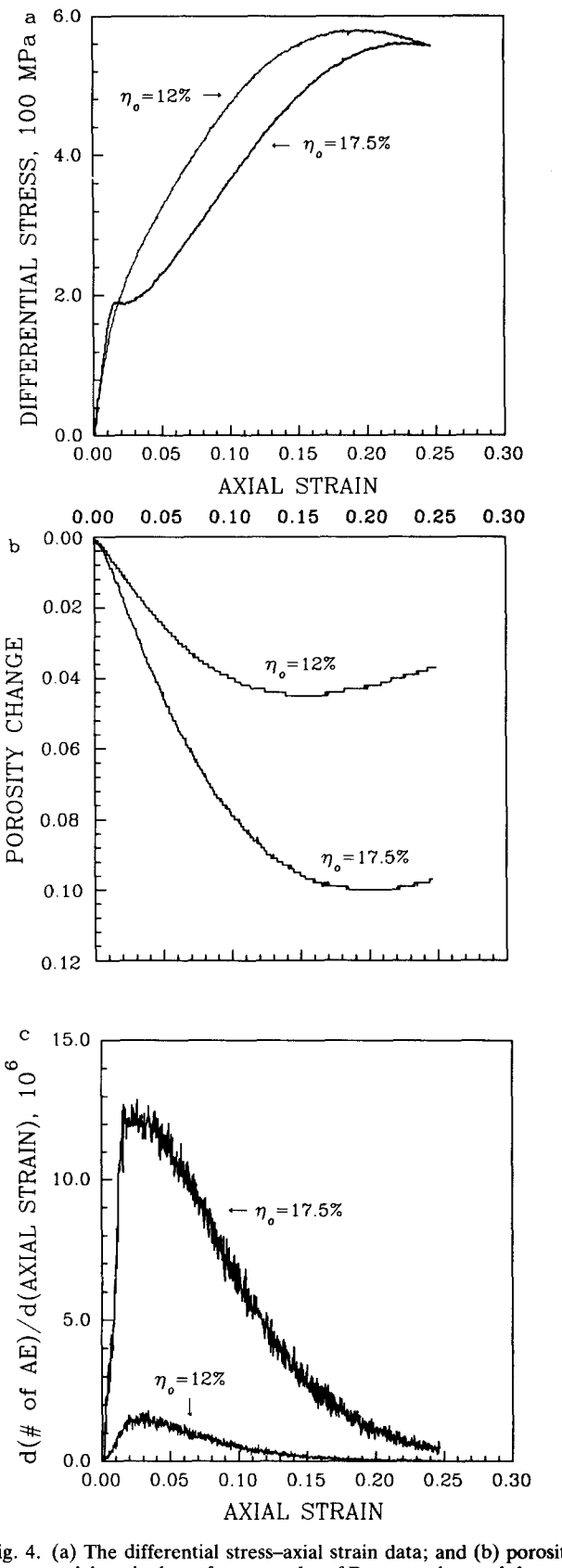

Fig. 4. (a) The differential stress–axial strain data; and (b) porosity change–axial strain data of two samples of Berea sandstone deformed at an effective pressure of 250 MPa. The overconsolidated sample BER4 had an initial porosity of 12%, and the normally consolidated sample BER2 had an initial porosity of 17.5%; (c) AE rate as a function of the axial strain of two Berea samples, BER2 and BER4, deformed at an effective pressure of 250 MPa.

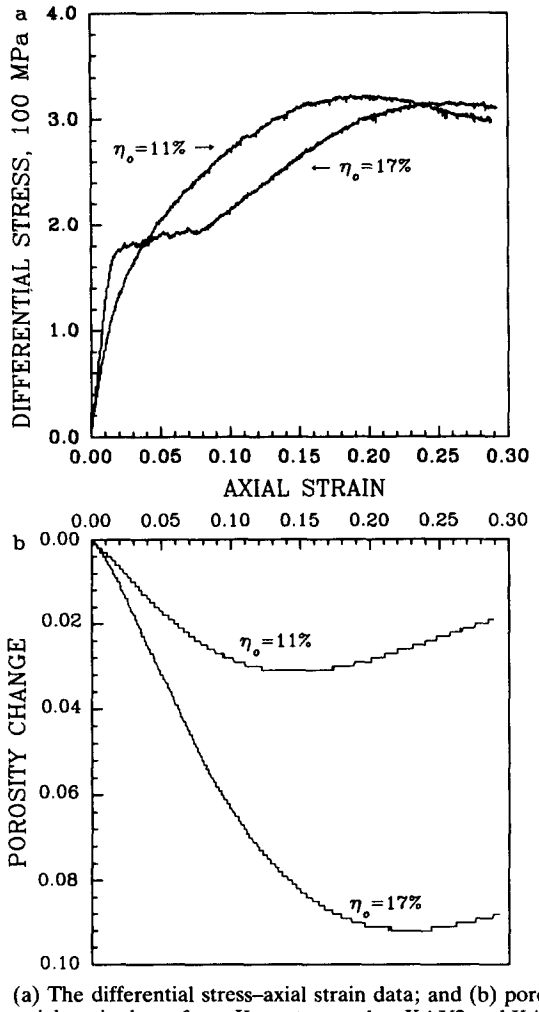

Fig. 5. (a) The differential stress–axial strain data; and (b) porosity change–axial strain data of two Kayenta samples, KAY2 and KAY3, deformed at an effective pressure of 150 MPa. The overconsolidated sample KAY3 had an initial porosity of 11%, and the normally consolidated sample KAY2 had an initial porosity of 17%.

Micromechanics of deformation

Acoustic emission measurements were performed during selected triaxial tests on Berea samples. Figures 2(c) and 4(c) show the relationship between the AE rate (the number of AE per unit strain) and the imposed axial strain. At an effective pressure of 40 MPa, the AE activity showed features very similar to those of a brittle, low porosity crystalline rock (Scholz 1968). Initially, the AE rate underwent a steady increase with increasing stress level. This continued until just before the peak stress was reached, at which point a very sudden acceleration of AE activity occurred. The sudden increase in AE activity is believed to be associated with the development of shear localization accompanied by an unstable stress drop. Following the major AE peak, there were several minor AE peaks observed. These are believed to be associated with small stress drops during sliding along the faulted band, although stress drops were not clearly indicated in the axial stress–stain data.

Although shear localization was evident in BER4 and BER3, the AE activities of these two brittle samples were quite different from those of BER1. The AE rate increased monotonically with the stress and reached a peak value during early stage of hardening, after which the AE rate decreased with further deformation. The development of shear localization in these two samples was not associated with any enhanced AE activity. In fact, the levels of AE activity during the dilatancy and post-failure stage were much lower than that during the hardening stage when the samples were subjected to compaction. The AE activity of ductilely deformed sample BER2 is similar to that observed in BER3 and BER4. In each of those samples the AE rate increased initially up to a peak value at relative small strain (of less than 2%) and then decreased with further deformation (Figs. 2c and 4c).

DISCUSSION

Transition maps

In this study, we have focused on the brittle–ductile transition in porous rocks. We propose three criteria to separate the inelastic behavior and the failure mode into two separate fields in a transition map in terms of effective pressure vs initial porosity. These are: (1) the inelastic behavior—whether the sample shows dilatancy or persistent compaction; (2) whether it shows strain softening or persists with constant yield and hardening; and (3) the failure mode—whether it develops shear localization or homogeneously distributed cataclastic flow. Maps separating the brittle field from the ductile field in a two-dimensional space of effective confining pressure and initial porosity are shown in Fig. 6(a) for Kayenta sandstone and Fig. 6(b) for Berea sandstone. These brittle–ductile transition maps were constructed on the basis of our deformation data as well as previously published deformation data (Handin *et al.* 1963, Jamison & Teufel 1979, Jones 1980, Bernabe & Brace 1990). On one side of the boundary separating brittle and ductile behavior with low effective pressure or low initial porosity, the inelastic deformation is accompanied by dilatancy and strain softening and the failure mode is by shear localization. On the other side of the boundary, with high effective pressure or high initial porosity, the failure process is ductile. Thus, the development of dilatancy and shear localization are both promoted by low initial porosities and low effective confining pressures.

Since we presented our data on Kayenta sandstone (Zhang *et al.* 1987, Wong 1990), several related studies on the effect of porosity on the brittle–ductile transition have been conducted. Focusing on sandstones of different porosities, Scott & Nielson (1991) used our approach to map out the brittle–ductile transition in the effective pressure–porosity space. A comprehensive compilation of laboratory data on the influence of porosity on the low-temperature brittle–ductile transition in siliciclastic rocks was recently presented by Rutter & Hadizadeh (1991).

Based on our transition maps, high pressure embrittlement could occur when the effect of porosity decrease

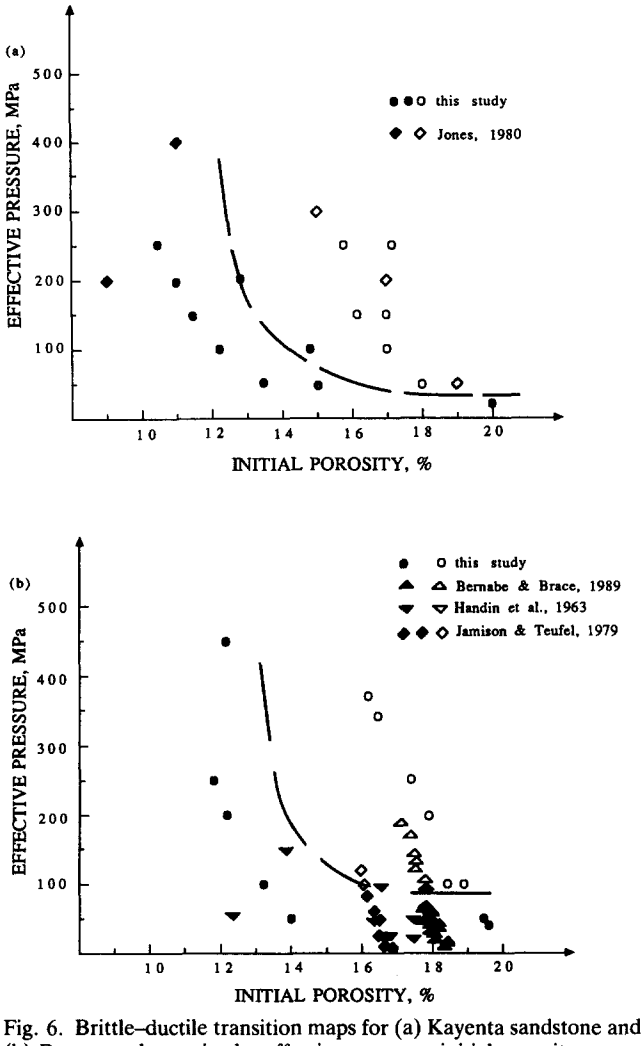

Fig. 6. Brittle–ductile transition maps for (a) Kayenta sandstone and (b) Berea sandstone in the effective pressure–initial porosity space. Solid symbols represent brittle behavior, open symbols represent homogeneous, macroscopically ductile deformation and lightly shaded symbols represent intermediate behavior. Note that the data from previous studies on Berea sandstone showed only the pressure effect on the transition of normally consolidated samples.

dominates over the effect of elevated pressure in controlling a rock location with respect to the transition. As shown by our high pressure embrittlement data for sample BER3 in the transition map (Fig. 6b), although elevated pressure promotes ductile behavior, the sample experienced significant porosity reduction due to hydrostatic loading up to 450 MPa (Fig. 2d) with an initial porosity of 10.5%. Having been subjected to hydrostatic compaction with porosity loss, the failure mode shifted to the brittle side of the boundary. Thus, high pressure embrittlement may in reality reflect the dependence of failure mode upon both pressure and porosity, rather than pressure alone.

Comparison of the transition maps (Fig. 6) from Berea and Kayenta sandstones shows that the transition boundary obtained from Berea sandstone is somewhat higher than that from Kayenta sandstone in the direction of increase of porosity and pressure. This discrepancy between the two boundaries suggests that in addition to the major effects from porosity and effective pressure, secondary effects, such as degree of lithification of porous rocks, may be involved. The Berea sandstone we used is highly cemented compared to the Kayenta sandstone, implying that the increase in the degree of lithification may promote brittle behavior. Some other factors not investigated here, including the angularity, size of grains and lithology may have additional effects. In particular, clay content may be important.

In a companion paper (Zhang *et al.* 1992), we present a similar transition map from Ocean Drilling Program Leg 131 core sediments (tuff) from Nankai accretionary wedge. The core volcanic sediments in a range of porosities from 25 to 40%, which is more porous than the sandstones in this study, were tested under effective pressures from 2 to 20 MPa which is within the pressure range to which the sediments from the toe of Nankai prism are expected to be subjected. The comparison between this transition map and the porosity data from Leg 131, most of which are located in the ductile zone, clearly indicates that the overall deformation of the sediments is dominantly ductile. The presence of discrete or brittle deformation at the toe of the Nankai prism is indicated by the documented occurrence of discrete faults, shear bands and zones of breccia and scaly fabric. We speculate that this brittle deformation is due to locally induced high pore pressure in excess of hydrostatic which can reduce effective pressure by an amount sufficient to shift the failure mode across the transition boundary from the ductile to the brittle zone.

Tectonic implications

The brittle and ductile behaviors we have observed are not to be regarded, respectively, as exactly equivalent to seismic and aseismic deformations. The localized deformation in the brittle zone can be either stable or unstable. Brace & Byerlee (1966) suggested that stick–slip instability in the laboratory provides a physical analogue for crustal earthquakes. Based on two earthquake instability models, the slip-weakening model of Rudnicki (1977) and the rate-state sensitive friction model of Dieterich (1979) and Ruina (1983), the instability would occur if the strain softening slope of the fault zone materials is steeper than the unloading stiffness of the surrounding materials, or if the fault zone material is velocity weakening and the stiffness of the loading system is below a critical stiffness. Therefore, the brittle behavior is a necessary, but not sufficient, condition for a runaway instability. The onset of such an instability also depends on the tectonic loading, material properties and elastic coupling to the surrounding material. However, on the other side of the transition map associated with ductile behavior, the occurrence of an earthquake instability can be ruled out due to the absence of shear localization and strain-softening.

The general porosity range of the transition to strain-localization in the clay-poor rocks we have studied is somewhere between 13 and 16% at an effective pressure of 100 MPa, which corresponds to the typical depth of the transition to seismic slip (12–16 km) with pore-fluid pressures intermediate between hydrostatic and litho-

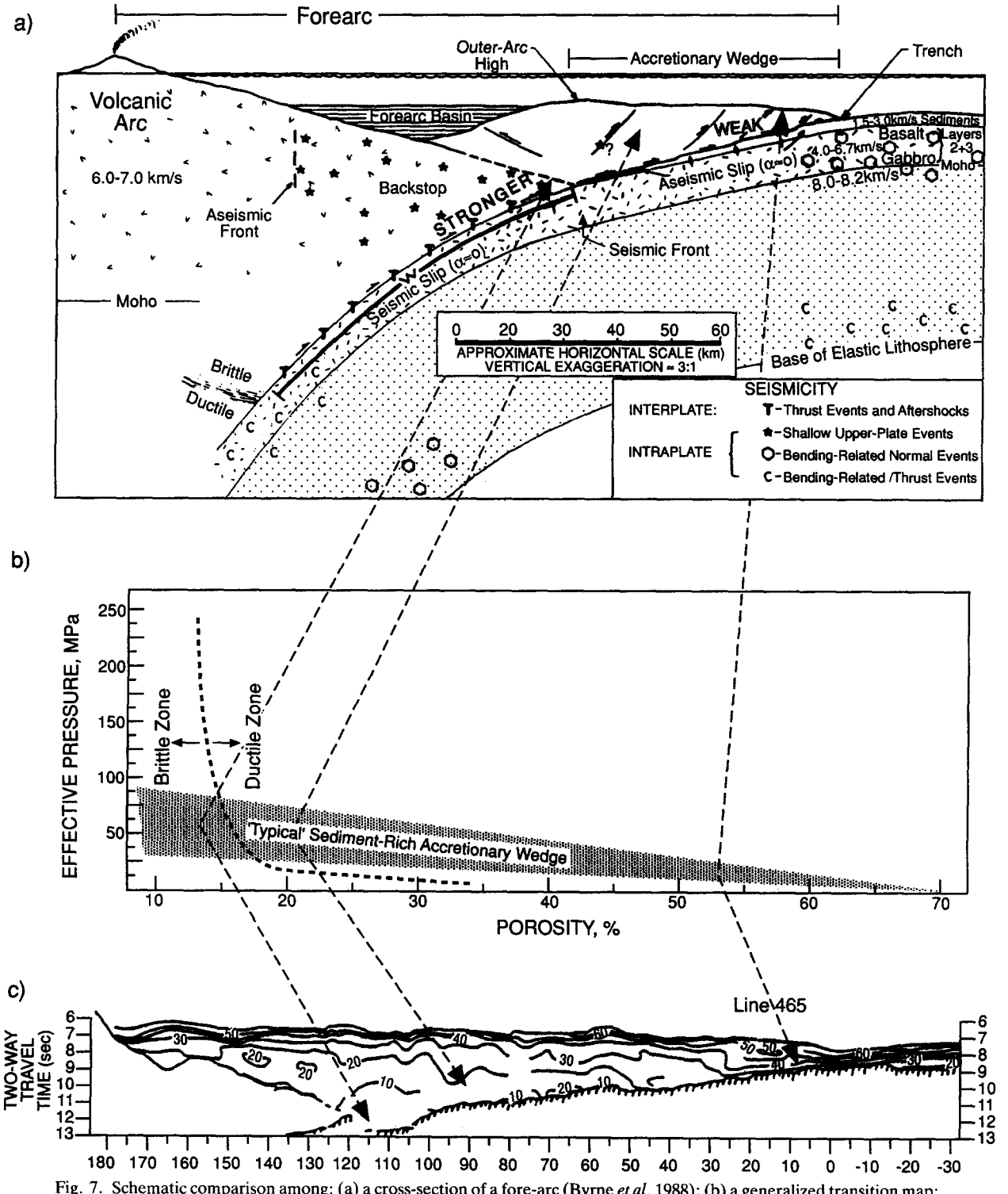

Fig. 7. Schematic comparison among: (a) a cross-section of a fore-arc (Byrne *et al.* 1988); (b) a generalized transition map; and (c) inferred porosity profile along a seismic reflection line in the Lesser Antilles fore-arc (Bangs *et al.* 1990).

static. The transition pressure would be lower with a higher porosity. In the ODP samples from the Nankai trough, the transition pressure could be as low as 2 MPa with a porosity of 40%. Figure 7(a) is a schematic cross-section of a fore-arc (Byrne *et al.* 1988). Figure 7(b) is a generalized, schematic transition map for clay-poor rocks, based upon the maps shown in Fig. 6. The stippled band represents an estimate of the suite of porosity–effective stress likely to be found along a line heading down-dip from the deformation front along the base of an accretionary wedge. Figure 7(c) is the porosity along a seismic reflection line in the Lesser Antilles fore-arc as inferred by Bangs *et al.* (1990). Lines are drawn connecting points within that band on the transition map to points in space, illustrated in Figs. 7(a) & (c).

Because seismic slip is unlikely in parts of an accretionary wedge falling to the right of the failure mode

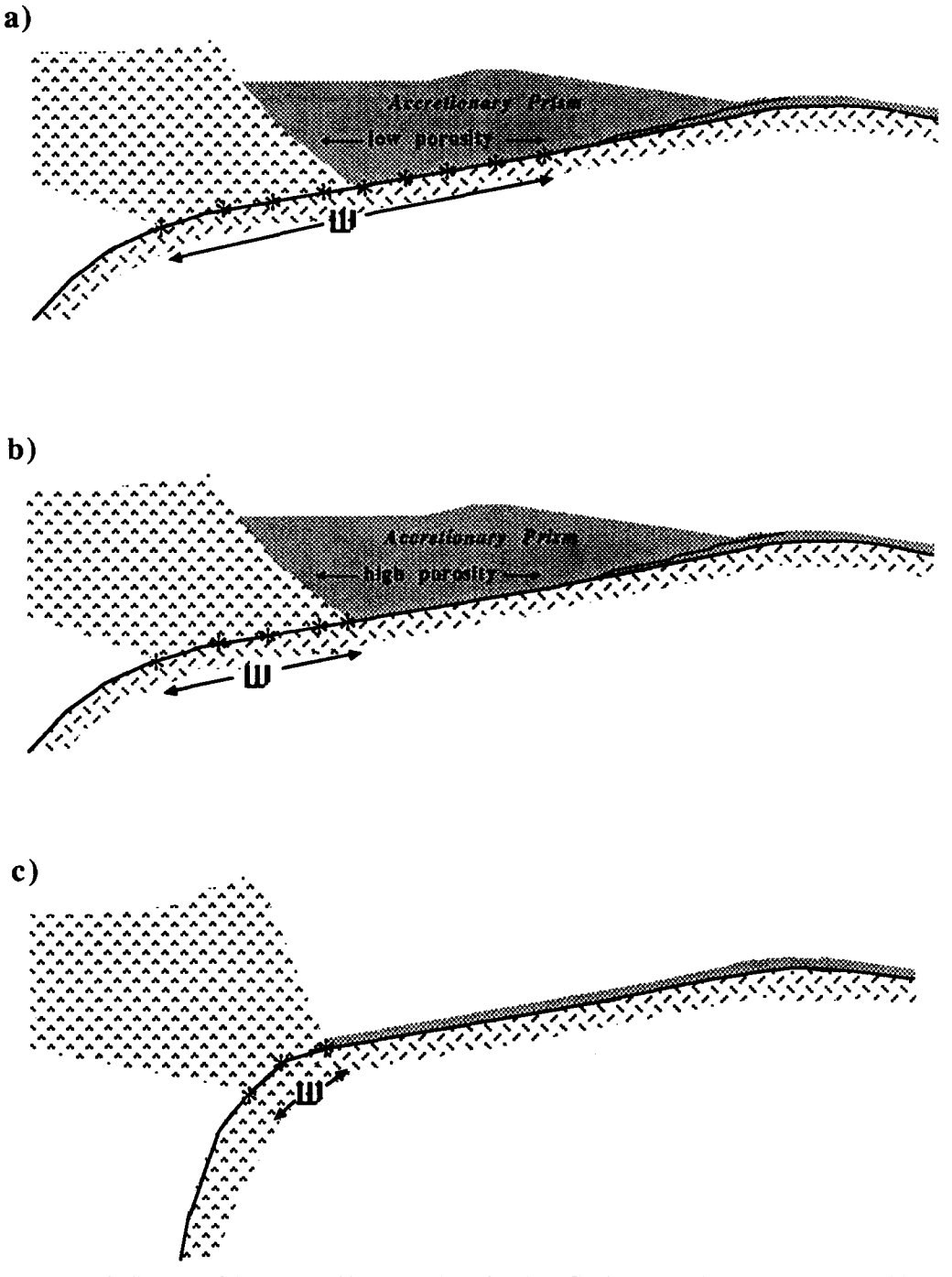

Fig. 8. Schematic diagrams of three types of fore-arcs where the widths W of seismogenic zones are different. (a) Type I: a sediment-rich accretionary prism has a wide plate contact zone. The sediments are well-compacted and well-lithified and they are capable of supporting seismic slip in great earthquakes along the broad plate boundary. (b) Type II: in contrast to type I, the sediments are relatively porous and they are not capable of deforming brittlely. Therefore, the width W of the seismogenic zone is very narrow although the plate contact zone is very wide. (c) Type III: the absence of accreted sediments makes the plate contact zone very narrow. Therefore, great earthquakes are not expected from this type of margins.

transition on a transition map, we suggested that accretionary wedges are aseismic because they are located in the ductile zone in porosity–effective stress space.

In reality, the situation is more complicated than that statement would imply. We do not consider healing effects, which may be important. A shear zone can be locally overpressured, which will tend to make it brittle, even if the surrounding sediments are predominantly ductile. We suggest (Zhang *et al.* 1992) that this effect explains the existence of discrete faults in the otherwise ductile toe region of the Nankai accretionary wedge.

An additional complication in estimating the location of the seismic front is the lithologic complexity of fore-arcs. Different types of sediments may have different transition maps, and the lithologic breakdown of the sedimentary assemblage deep within the wedge, beyond the reach of drilling, is not generally well known. Furthermore, as illustrated in Fig. 7, the downgoing plate eventually encounters a backstop. Although in some cases a backstop is simply older and better lithified accreted sediment, at other margins (such as Lesser Antilles) it appears to consist of igneous basement

(Westbrook 1975, Bangs *et al.* 1990). If the porosity–effective pressure conditions within the accretionary wedge never reach those required for seismic slip, then the entire accretionary wedge may be aseismic and plate-boundary thrusting earthquakes may begin only where basement rocks reach the downgoing plate (Byrne *et al.* 1988).

Ruff (1989) has shown the existence of a strong correlation between large earthquakes and the presence of 'excess sediments', which he defines as the presence of an accretionary wedge and the absence of the horst-and-graben structures characteristic of sediment-starved subduction zones. However, we suggest that the important factor is not merely the presence or absence of large quantities of sediments, but rather their mechanical behavior. A long history of sediment accretion can lead to the development of an extremely wide zone of plate contact. If most of those sediments are compacted and well-lithified (as in Alaska and Chile), then it is possible that they can undergo seismic slip in extremely large earthquakes along the broad plate boundary that their accretion has created (Fig. 8a). However, if the sediments are still relatively porous, then they may be aseismic and even very broad fore-arcs may not produce great earthquakes (Fig. 8b). Examples of this sort of margin are difficult to determine, given the possibility that the lack of large recorded events may simply indicate a long interseismic period between great earthquakes. Possible examples of margins with large quantities of sediment that have built a broad zone of plate contact but might not produce great earthquakes because of the poorly consolidated nature of most of those sediments are western Makran, the southern Lesser Antilles and Cascadia. Margins that have little or no accreted sediment generally have a very narrow zone of plate contact and should not be expected to produce great earthquakes (Fig. 8c).

The role of sediments in influencing the maximum size of plate-boundary thrusting earthquakes is not simple. However, it may be possible to make some useful generalization. First, lacking a long history of sediment accretion, a margin is unlikely to produce great earthquakes because the zone of plate contact is likely to be too narrow. Second, if the plate-boundary sediments are too young and undercompacted to be capable of brittle shear localization and stick–slip behavior, then great earthquakes can not occur, because slip along most of the boundary will be aseismic. However, great earthquakes are to be expected at margins that have a large plate contact consisting of rock that are generally capable of shear localization, brittle failure and stress drops.

Acknowledgements—This research project was supported by the National Science Foundation through grants OCE-8915473 (to D. M. Davis), EAR-8721045 (to D. M. Davis and T.-f. Wong) and EAR-8904146 (to T.-f. Wong). J. Zhang was also supported by a JOI/USSAC Ocean Drilling Fellowship. Comments by J. Hadizadeh and F. A. Dahlen have been very useful.

REFERENCES

Abe, K. 1975. Reliable estimation of the seismic moment of large earthquakes. *J. Phys. Earth* **23**, 381–390.

Bangs, N. B., Westbrook, G. K., Ladd, J. W. & Buhl, P. 1990. Seismic velocities from the Barbados ridge complex, indicators of high pore fluid pressures in an accretionary complex. *J. geophys. Res.* **95**, 8767–8782.

Bernabe, Y. & Brace, W. F. 1990. Deformation and fracture of Berea sandstone. In: *The Heard Volume. Am. Geophys. Un. Geophys. Monogr.* **56**, 91–101.

Brace, W. F. & Byerlee, J. D. 1966. Stick-slip as a mechanism for earthquakes. *Science* **153**, 990–992.

Brace, W. F., Silver, E., Hadley, K. & Goetze, C. 1972. A closer look at cracks and pores, *Science* **178**, 162–163.

Byrne, D. E., Davis, D. M. & Sykes, L. R. 1988. Loci and maximum size of thrust earthquakes and the mechanics of the shallow region of subduction zones. *Tectonics* 7, 833–857.

Byrne, D., Sykes, L. R. & Davis, D. M. In press. Great thrust earthquakes and aseismic slip along the plate boundary of the Makran subduction zone. *J. geophys. Res.*

Chapple, W. M. 1978. Mechanics of thin-skinned fold-and-thrust belts. *Bull. geol. Soc. Am.* **89**, 275–304.

Chen, A. T., Frohlich, C. & Latham, G. V. 1982. Seismicity of the forearc marginal wedge (accretionary prism). *J. geophys. Res.* **87**, 3679–3690.

Curran, J. H. & Carroll, M. M. 1979. Shear stress enhancement of void compaction. *J. geophys. Res.* **84**, 1105–1112.

Davis, D. M. & Hussong, D. M. 1984. Geothermal observations during Deep Sea Drilling Project Leg 78A. *Init. Reps DSDP* **78A**, 593–598.

Davis, D. M., Suppe, J. & Dahlen, F. 1983. Mechanics of fold-and-thrust belts and accretionary wedges. *J. geophys. Res.* **88**, 1153–1172.

Dieterich, J. H. 1979. Modeling of rock friction, experimental results and constitutive equation. *J. geophys. Res.* **84**, 2161–2168.

Edmond, J. M. & Paterson, M. S. 1972. Volume change during the deformation of rocks at high pressure. *Int. J. Rock Mech. & Min. Sci.* **9**, 161–182.

Evans, B, Fredrich, J. T. & Wong, T.-f. 1990. The brittle–ductile transition in rocks, recent experimental and theoretical progress. In: *The Heard Volume. Am. Geophys. Un. Geophys. Monogr.* **56**, 1–20.

Fredrich, J. T., Evans, B. & Wong, T.-f. 1989. Micromechanics of the brittle to plastic transition in Carrara marble. *J. geophys. Res.* **94**, 4129–4145.

Handin, J., Hager, R. V., Friedman, M. & Feather, J. N. 1963. Experimental deformation of sedimentary rock under confining pressure, pore pressure effects. *Bull. Am. Ass. Petrol. Geol.* **47**, 717–755.

Heard, H. C. 1960. Transition from brittle fracture to ductile flow in Solnhofen limestone as a function of temperature, confining pressure and interstitial fluid pressure. In: *Rock Deformation. Mem. geol. Soc. Am.* **79**, 193–226.

Hirth, G & Tullis, J. 1989. The effects of pressure and porosity on the micromechanics of the brittle–ductile transition in quartzite. *J. geophys. Res.* **94**, 17,825–17,838.

Jamison, W. R. & Teufel, L. W. 1979. Pore volume changes associated with failure and frictional sliding of a porous sandstone. *Proc. U.S. Symp. Rock Mech.* **20**, 163–170.

Jones, L. M. 1980. Cyclic loading of simulated fault gouge to large strains. *J. geophys. Res.* **85**, 1826–1832.

Kanamori, H. 1986. Rupture process of subduction zone earthquakes. *Annu. Rev. Earth Sci.* **14**, 293–322.

Lundberg, N. & Moore, J. C. 1986. Macroscopic structural features in Deep Sea Drilling Project cores from forearc regions. *Mem. geol. Soc. Am.* **166**, 13–44.

Moore, J. C. & Biju-Duval, B. 1984. Tectonic synthesis, Deep Sea Drilling Project Leg 78A: structural evolution of offscraped and underthrust sediment. Northern Barbados Ridge complex. *Init. Reps DSDP* **78A**, 601–621.

Moore, J. C., Roeske, S., Lundberg, N., Schoonmaker, J., Cowan, D. S., Gonzales, E. & Lucas, S. E. 1986. Scaly fabrics from Deep Sea Drilling Project cores from forearcs. *Mem. geol. Soc. Am.* **166**, 55–73.

Paterson, M. S. 1976. *Experimental Rock Deformation–The Brittle Field.* Springer, New York.

Rudnicki, J. W. 1977. The inception of faulting in a rock mass with a weakened zone. *J. geophys. Res.* **82**, 844–854.

Ruff, L. J. & Kanamori, H. 1980. Seismicity and the subduction process. *Phys. Earth & Planet. Interiors* **23**, 240–253.

Ruff, L. J. 1989. Do trench sediments affect great earthquake occurrence in subduction zones? *Pure & Appl. Geophys.* **129**, 263–282.

Ruina, A. L. 1983. Slip instability and state variable friction laws. *J. geophys. Res.* **88**, 10,359–10,370.

Rutter, E. H. & Hadizadeh, J. 1991. On the influence of porosity on the low-temperature brittle–ductile transition in siliciclastic rocks. *J. Struct. Geol.* **13**, 609–614.

Scholz, C. H. 1968. Microfracturing and the inelastic deformation of rock in compression. *J. geophys. Res.* **73**, 1417–1432.

Scott, T. E. & Nielsen, K. C. 1991. The effects of porosity on the brittle–ductile transition in sandstone. *J. geophys. Res.* **96**, 405–414.

Shipboard Scientific Party 1991. Site 808. *Init. Reps ODP* **131**, 71–269.

Sondergeld, C. H. 1980. Effective noise discriminator for use in acoustic emission studies. *Rev. Sci. Instrum.* **51**, 1342–1344.

Stockmal, G. S. 1983. Modeling of large scale accretionary wedge deformation. *J. geophys. Res.* **88**, 8271–8287.

Tullis, J. & Yund, R. A. 1977. Experimental deformation of dry Westerly granite. *J. geophys. Res.* **82**, 5705–5718.

Vrolijk, P. 1990. On the mechanical role of smectite in subduction zones. *Geology* **18**, 703–707.

Westbrook, G. K. 1975. The structure of the crust and upper mantle in the region of Barbados and the Lesser Antilles. *Geophys. J. R. astr. Soc.* **43**, 201–242.

Wong, T.-f. 1990. Mechanical compaction and brittle–ductile transition in porous sandstones. In: *Deformation Mechanisms, Rheology and Tectonics* (edited by Knipe, R. J. & Rutter, E. H.). *Spec. Publs geol. Soc. Lond.* **54**, 111–122.

Zhang, J., Davis, D. M. & Wong, T.-f. 1992. Failure modes of tuff samples from leg 131 in Nankai accretionary wedge. *Proc. Ocean Drilling Program, Scient. Results* **131**.

Zhang, J., Wong, T.-f. & Davis, D. M. 1990a. Micromechanics of pressure-induced grain crushing in porous rocks. *J. geophys. Res.* **95**, 341–352.

Zhang, J., Wong, T.-f. & Davis, D. M. 1990b. High pressure embrittlement and shear-enhanced compaction of Berea sandstone, Acoustic emission measurement and microstructural observation. In: *Rock Mechanics Contributions and Challenges, Proc. of 31st U.S. Symposium* (edited by Hustrulid, W. A. & Johnson, G. A.). A. A. Balkems, Rotterdam, 653–660.

Zhang, J., Wong, T.-f., Yanagidani, T. & Davis, D. M. 1990c. Pressure-induced microcracking and grain crushing in Berea and Boise sandstones, acoustic emission and quantitative microscopy measurements. *Mech. Mater.* **9**, 1–15.

Zhang, J., Wong, T.-f. & Davis, D. M. 1987. Failure mode as a function of porosity and effective pressure in porous sandstones. *Geol. Soc. Am. Abs. w. Prog.* **19**, 904.

Zhao, W. L., Davis, D. M., Dahlen, F. A. & Suppe, J. 1986. Origin of convex accretionary wedges, evidence from Barbados. *J. geophys. Res.* **91**, 10,246–10,258.